# Infrared Sensitivity of Plasmonic Metal Films with Hole Arrays to Microspheres In and Out of the Holes

**ARTICLE** *in* THE JOURNAL OF PHYSICAL CHEMISTRY C · DECEMBER 2010

Impact Factor: 4.77 · DOI: 10.1021/jp908897z

# Infrared Sensitivity of Plasmonic Metal Films with Hole Arrays to Microspheres In and Out of the Holes

**Joseph Heer, Lloyd Corwin, Katherine Cilwa, Marvin A. Malone, and James V. Coe***

*Department of Chemistry, The Ohio State University, 100 West 18th Avenue, Columbus, Ohio 43210-1173*

*Received: September 14, 2009; Revised Manuscript Received: November 03, 2009*

Both experiments and finite difference time domain (FDTD) calculations show that infrared (IR) absorption spectroscopy and IR transmission resonances of metal films with arrays of subwavelength holes (meshes) are more sensitive to material in the holes of the mesh than to material on the front or back surfaces of the mesh. IR extinction spectra of isolated, individual latex (polystyrene) spheres inside or outside of a hole on plasmonic Ni mesh are compared to similar isolated microspheres on a ZnSe substrate. Although vibrational spectra of single microspheres on ZnSe are dominated by scattering, vibrational spectra of microspheres in microholes of metal mesh are dominated by absorption. The IR absorption spectrum of a latex microsphere with mesh is much stronger when the microsphere is inside a mesh hole rather than on the front or back surface, which pertains to the nature of spectroscopic enhancements on the plasmonic mesh. These results are supported and enhanced by FDTD simulations showing changes in the primary infrared transmission resonance of the mesh when latex spheres are placed in different positions. The simulations demonstrate how interaction with a plasmonic resonance changes the intensity and line shape of a vibration in the dielectric material.

## 1. Introduction

The availability of latex spheres, with specific, well-controlled diameters on the scale of the wavelength of incident light, has spurred many applications in microtechnology, nanotechnology, and plasmonics.[1,2] Tiny spheres are short-focal-length lensing elements that can be coated with metal to produce subwavelength plasmonic structures.[3,4] They exhibit resonances associated with multiple reflections within the sphere, such as whispering gallery modes,[2,5] and have been used as microlasers.[6] Placing an individual latex microsphere into a metal microchannel affects the infrared (IR) spectral properties of both the metal film and the microsphere. The metal film containing the microchannel is thinner than the microsphere's diameter, so the arrangement is like adding a metal belt to the microsphere; that is, some light that would be lost to scattering by an isolated microsphere is redirected back into the microsphere. Plasmonic metal films with arrays of subwavelength holes (mesh) are the subject of great current interest (optical metamaterials[7−9] and subwavelength optics[10−15]) due, in part, to surface plasmon (SP) mediated optical properties. Reviews of the field of metal mesh arrays,[12,15−17] including the plasmonic properties of metal films[16] and our own work on metal meshes,[18] are available for those interested in more background.

Airborne particles in the 1−5 $\mu$m size regime are particularly important to people because these are the largest globular particles that get past our noses and throats and make it into the lungs.[19] This work is partly motivated by the desire to apply IR absorption spectroscopy to the chemical identification of such particles. Acquisition of vibrational spectra of individual, wavelength-scale particles has several problems, including (1) objects of this size (like dust, cells, spores, and aerosols) scatter IR light very efficiently such that scattering dominates absorption and (2) very little IR radiation is transmitted when the window is reduced to the size of these particles. Investigators can use IR radiation from expensive, high-energy synchrotron sources[20−22] (with ∼1000 times more power than desktop FTIRs) to beat the latter problem; however, they are still subject to the first problem. Plasmonic metal mesh offers a simple and inexpensive means to beat both problems. In this work, the IR extinction spectra of single, isolated, 5 $\mu$m diameter latex (polystyrene) spheres are recorded and compared under the variations shown in Figure 1 (isolated on a ZnSe substrate, accommodated within a single 5 $\mu$m wide metal microchannel, or on the front surface of the mesh outside of a metal microchannel). Several recent studies have suggested the importance of materials in the holes of the mesh,[23−25] so experiments placing materials specifically in the holes are timely and technologically relevant. The conclusions of our experiments are reinforced with FDTD simulations of the IR transmission spectra of periodic mesh/microsphere structures, including both the effects of microspheres in and outside of the holes and the addition of a vibrational feature to the dielectric function used to model the microsphere material.

## 2. Methods

The mesh is Ni with a square pattern of square holes (12.6 $\mu$m lattice parameter, square holes with a width of ∼5.0 $\mu$m and a thickness of ∼2 $\mu$m) and was obtained from Precision Eforming LLC (839 Route 13, Courtland, NY 13045, www.precisionforming.com, part no. MN47). The latex microspheres fit tightly in the mesh holes, are polystyrene, have an index of refraction of 1.58 (at 540 nm), and have a specified diameter of 5.0 ± 0.4 $\mu$m. They were obtained from SPI Supplies (P.O. Box 656, West Chester, PA, 19381-0656, www.2spi.com, product no. 02705-AB, lot no. 1120920) and come in a 1% aqueous suspension of uniform polystyrene DVB microspheres in deionized water with 0.1% $NaN_3$ and a proprietary surfactant. Samples on ZnSe and Ni mesh were prepared by evaporation of a small drop of commercial aqueous suspension on the substrates, which leaves a macroscopic ring of microspheres on the surface at the original edge of the drop. Once dry, a

* To whom correspondence should be addressed. E-mail: coe.1@osu.edu.

10.1021/jp908897z 
Published on Web 12/03/2009

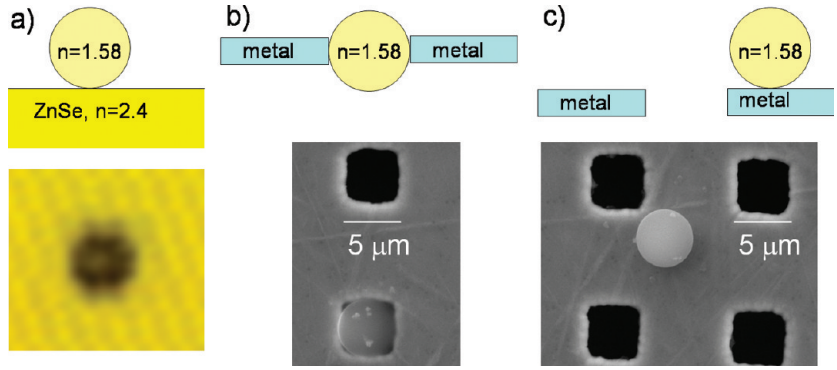


**Figure 1.** IR extinction spectra of individual 5 $\mu$m diameter latex spheres were recorded for different situations: (a) a sphere on a ZnSe window substrate shown schematically above with an optical microscope image below, (b) a sphere in a microchannel of the metal mesh with a scanning electron microscope (SEM) image below, and (c) a sphere on the front side of the metal mesh, i.e., not in a hole (SEM image below).

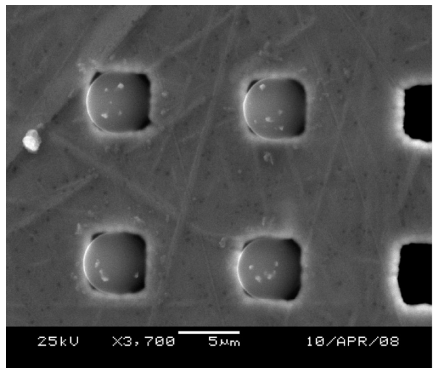


**Figure 2.** SEM image, at ~40° to the $e^-$ beam, of four individual 5 $\mu$m diameter latex spheres, stuck in the ~5.0 $\mu$m holes of the Ni mesh. The white specs on the microspheres are azide nanocrystals.

drop of distilled water is applied (to dissolve surfactant and azide) and removed with a corner of a Kimwipe. After drying again, a drop of water is added and spread around the mesh with a glass capillary. This process breaks up the ring and seems to draw spheres into the mesh microchannels as the drop evaporates. Regions with high concentrations of microspheres in microchannels can be produced with several spread-drop treatments. An SEM (JEOL JSM-5500 instrument) of this arrangement is shown in Figure 2. One 84-hole region had 33 microspheres sucked into holes and only 12 microspheres on the front surface, as assayed by SEM.

Extinction spectra were recorded of individual, isolated microspheres using a PerkinElmer Spectrum Spotlight 300 FTIR imaging microscope system in both imaging and point mode. In imaging mode, the operator chooses a rectangular microregion and full FTIR spectra were recorded at every point on a 6.25 $\mu$m square lattice within the region using an array of 16 $N_2$(l)-cooled MCT detectors. In point mode, the operator chooses a microregion and obtains a single FTIR spectrum with a single $N_2$(l)-cooled MCT detector. Typical operating conditions included a range of 4000−680 $cm^{-1}$ (stretching the commercially specified lower range of 720 $cm^{-1}$) with 4 $cm^{-1}$ resolution. Backgrounds were recorded in regions of the substrate (ZnSe or mesh) without microspheres. The microspectrometer has a Cassegrain optical system that exposes samples to a cone of radiation at angles of 17−37° from the center ray. This extensively disperses mesh transmission resonances by comparison to the nominal 0° incident angle in a normal, benchtop FTIR.[26]

Sphere and mesh simulations were accomplished using FDTD 6.0 electromagnetic simulation software from Lumerical Inc. (Vancouver, BC, www.lumerical.com). The program solves the differential form of Maxwell's equations at a series of time steps based on the Yee methodology[27] with a user-specified grid and cell configuration. The simulations generally send a polarized, planar pulse of light toward a mesh (or sphere), measuring the light transmitted using a detector on the other side. The light pulse is tailored using Fourier transform techniques to cover a specified region of the mid-IR. The simulation cell region for mesh simulations was usually 60 $\mu$m in the direction of incident light propagation. Typically, a two-dimensional mesh unit cell, 12.7 $\mu$m by 12.7 $\mu$m, was arranged perpendicular to the incident light in the middle of the cell. The simulation cell had absorbing (PML) boundary conditions at the beginning and ends of the propagation direction, symmetric boundary conditions along the sides parallel to the light's polarized E-field, and antisymmetric boundary conditions on the sides perpendicular to the light's polarized E-field. These constraints reduced time and memory requirements by a factor of 4 over standard periodic boundary conditions. The background was taken as air ($\varepsilon = n = 1$), and Ni mesh was modeled as a 2 $\mu$m thick film based on Palik's Ni dielectric function,[28] perforated by a square pattern of square holes. The holes were 5.0 $\mu$m by 5.0 $\mu$m squares with a 12.7 $\mu$m lattice parameter (hole center-to-hole center distance). The latex microspheres were modeled as 5.0 $\mu$m diameter spheres with a dielectric permittivity of $\varepsilon = 2.45862$ ($n = 1.568$). Gridding was nonuniform and based on the local material permittivity ("auto-non-uniform" option), with a medium accuracy ("3") in the metal skin (0.1 $\mu$m skin depth), air, and latex. To reduce computation time, the grid resolution was lowered ("override index" = 1 option) in the bulk metal where there was little field strength. Time spans were typically 30 000 fs with a step size of 0.0366 fs, which required ~3 h on a PC with the Microsoft Windows Vista Business 64 bit operating system (Intel Core 2 Quad Processor Q9300 and 8GB DDR2-800 RAM). The ZnSe/sphere simulation region was 25 $\mu$m by 10 $\mu$m by 10 $\mu$m. Absorbing (PML) boundary conditions were used on all sides. A 5 $\mu$m latex microsphere ($n = 1.58$) was placed in contact with a constant dielectric material representing ZnSe ($n = 2.4$) that filled the latter half of the simulation region. Again, a polarized pulse of IR light was propagated parallel to the long axis, beginning in the ZnSe slab, passing through the latex sphere, and ending in air($\varepsilon = n = 1$).

## 3. Individual Microspheres on ZnSe

Large scattering effects arise when the diameter of a microsphere is similar to the wavelength of incident light. The most important features are predicted by Mie theory of isolated spheres, as presented by van de Hulst,[29] namely, a broad,

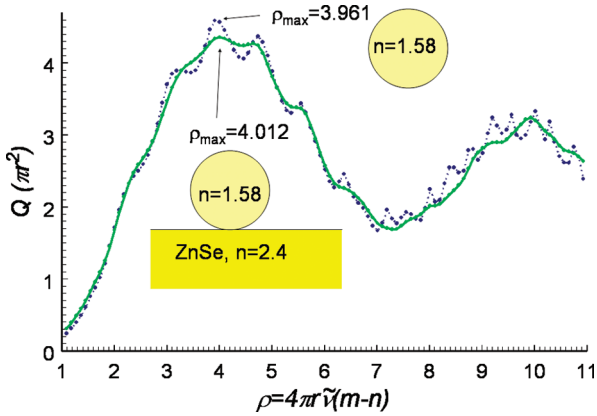


**Figure 3.** FDTD calculation of the extinction cross section (in units of particle area) of a 5 $\mu$m diameter latex sphere with (blue, dotted) and without (green, solid) a ZnSe surface as presented versus the reduced scattering parameter, which is proportional to wavenumbers.

scattering-dominated spectrum with finer oscillations (blue, dotted trace in Figure 3); however, such studies often ignore the effect of the substrate, which is difficult to treat analytically. FDTD calculations were used to compare scattering from an isolated 5-$\mu$m latex ($m = 1.58$) microsphere (blue, dotted trace in Figure 3) with scattering by a similar microsphere in contact with a flat ZnSe ($n = 2.40$) surface (green, solid trace of Figure 3.) The calculation was converted to van de Hulst's[29] reduced variable, $\rho = 4\pi r\tilde{\nu}(m - n)$, where $r$ is the radius of the particle, $\tilde{\nu}$ is the frequency of the light in wavenumbers, $m$ is the index of refraction of the microsphere, and $n = 1$ is the index of refraction of the surrounding space. The trace of the free microsphere (blue, dotted) is very similar to that presented by van de Hulst[29] (p 177 therein) and provides confidence in the FDTD calculations. The effect of the ZnSe surface is to reduce and broaden the higher frequency oscillations in the scattering cross section.

An optical microscope image of a 250 $\mu$m by 362.4 $\mu$m region on a ZnSe substrate with a variety of 5 $\mu$m diameter latex spheres (SPI, polystyrene, $n = 1.58$) is shown in Figure 4a, showing both clumps and isolated individuals. An IR imaging scan of this region was recorded (4 cm$^{-1}$ resolution, 512 scans, 4000−700 cm$^{-1}$ range, 6.25 $\mu$m pixel size, requiring 14.3 h). An image based on extinction at 2202 cm$^{-1}$ is given in Figure 4b (using a two-point baseline at 792 and 3963 cm$^{-1}$). Although the most prominent scattering occurs from clumps, 20 prospective single and isolated latex spheres were identified and labeled in the scattering image (Figure 4b). Four of these (4, 14, 15, 17) were eliminated from consideration as isolated single spheres because they were too close to other spheres or dust particles. Extinction spectra of the 16 remaining single particles were obtained by coadding transmission spectra on the 6.25 $\mu$m pixel grid within a 13 $\mu$m × 13 $\mu$m region centered on each single microsphere, using an empty adjacent region of identical size as background. The resulting extinction spectra are presented in Figure 5 with offsets for better viewing. The experimental single sphere spectra have features dominated by simple Mie scattering theory of isolated spheres,[30] namely, a broad scattering spectrum with finer oscillations. The oscillations are reduced and broadened from the predictions of Mie scattering of an isolated particle, but are reasonably well-modeled by the FDTD calculations for a microsphere on a ZnSe surface (red curve). The simulation curve presented in Figure 5 has the particle radius reduced by a factor of 0.94 over the manufacturer's specification (which may be due to differences between the model system of perpendicular incidence and the experimental Cassegrain optics). The van de Hulst's reduced variable representation allows the results of Figure 3 to be applied with fine adjustments without the need to repeat calculations. Noting that the FDTD calculations predict $\rho_{max} = 4.012$, the variations in the observed wavenumber values at maximum scattering intensity can be interpreted as due to variations in the radii of individual spheres. Under this assumption, a Gaussian standard deviation of 0.019 $\mu$m was found for the distribution of microsphere radii from this lot.

Most importantly for this work, the experimental spectra also have distinct vibrational features. The strongest of these are only about 10−20% as intense as the scattering, as can be better examined in Figure 6. Also, these features appear out-of-phase with pure absorption, which go up (as shown in black with the bottom trace). Such results are well-known[31] (e.g., the Christiansen effect[32]) and can be modeled by Mie theory[29] (p193 therein) to some extent. Because the latex sphere was modeled with a constant real value of the index of refraction, the FDTD calculations do not show vibrational features and should not be expected to match experiment exactly. Clearly, scattering dominates the extinction spectra of single microspheres on ZnSe.

## 4. Individual Microsphere In and Out of Hole in Metal Mesh

An individual, 5 $\mu$m diameter, latex sphere in a hole of the mesh at the center of a 16 pixel by 16 pixel region (6.25 $\mu$m/pixel) of mesh had spectra recorded in image mode with 256 scans/pixel (an optical microscope image of the central portion of the imaged region is shown in the top inset of Figure 7). All of the latex (polystyrene) vibrational features occurred in absorption, which stands in contrast to the results of microspheres on ZnSe. Absorbances at 3025 cm$^{-1}$ (aromatic C−H stretch) were collected from the spectra of grid points closest to the particle center, and a nonlinear least-squares fit to a 2-D Gaussian gave an intensity correction factor of 1.05 ± 0.13 to obtain the absorbance at the center of the microsphere. This correction was incorporated in the top trace of Figure 7, which also has the baseline flattened.

Two individual, 5 $\mu$m diameter, latex spheres, that were not in holes (see the inset optical image at the right of Figure 7), were within a 13 pixel by 6 pixel region (6.25 $\mu$m/pixel) of mesh and had spectra recorded twice in image mode for a total of 1024 scans/pixel. The resulting absorption traces were flattened and presented as the bottom two traces in Figure 7. The signals were not strong enough to provide fitted absorbances at the centers of the particles, but such corrections tend to lie in a range from 1 to 1.2. Using the aliphatic C−H stretch absorbance at 2926 cm$^{-1}$, the spectra of individual spheres not in the holes of mesh are ∼13 times weaker than the spectrum of a sphere in the hole.

Latex microspheres in holes also have a strong effect on the plasmonic transmission resonances of mesh. A region containing two microholes had transmission spectra recorded in point mode with both holes empty, one hole filled, and both holes filled with 5 $\mu$m diameter latex spheres. The transmission spectra are shown in Figure 8. The IR microscope has rays ranging from 17° to 37°, so there is a large range of $k$ values. The effect is to smear the plasmonic transmission resonances into a broad lump from ∼500 to 1500 cm$^{-1}$. The addition of latex spheres within the holes has a dramatic effect on this lump of resonances; they red shift and are attenuated, but the lack of resolution in $k$ limits the information that can be extracted. Note also how two latex spheres produce pronounced vibrational

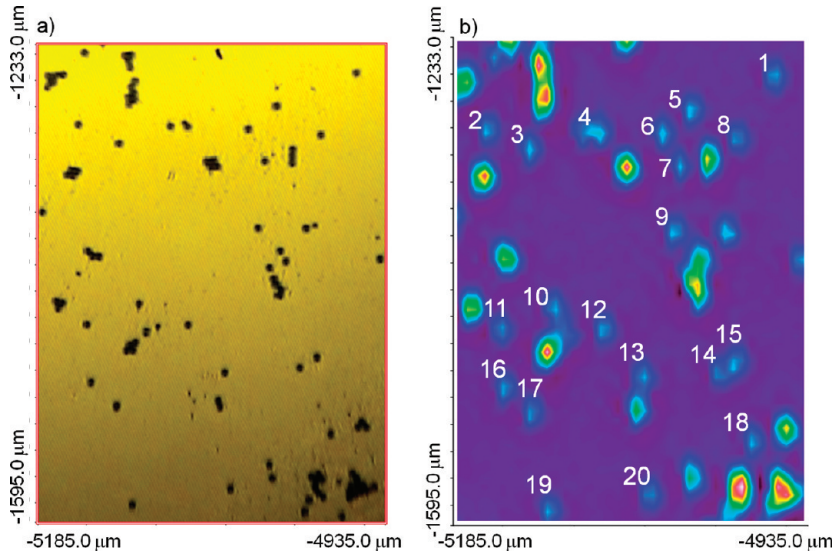


**Figure 4.** (a) Optical image of 5 $\mu$m diameter latex spheres on a ZnSe substrate. (b) Corresponding image of extinction at 2202 cm$^{-1}$, which is near the maximum in the scattering spectrum predicted by Mie theory.

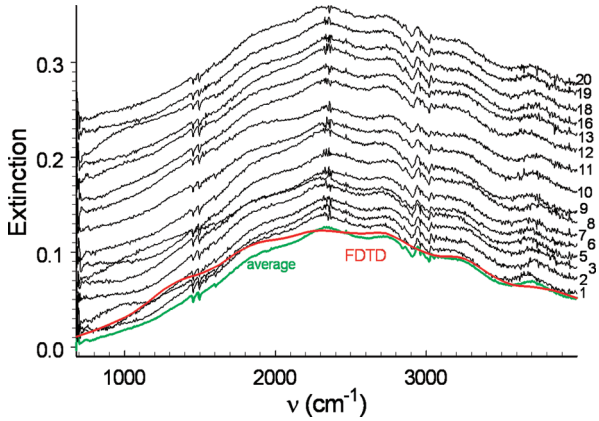


**Figure 5.** Extinction (absorption and scattering) spectra of individual 5 $\mu$m diameter latex microspheres, as numbered in Figure 4b. All of the individual spectra are offset for easier viewing, excepting the average spectrum of the 16 individuals (green). A scaled FDTD computation of the extinction spectrum of a single 5 $\mu$m diameter polystyrene sphere on a flat ZnSe surface (red) shows reasonable agreement with the observed spectra.

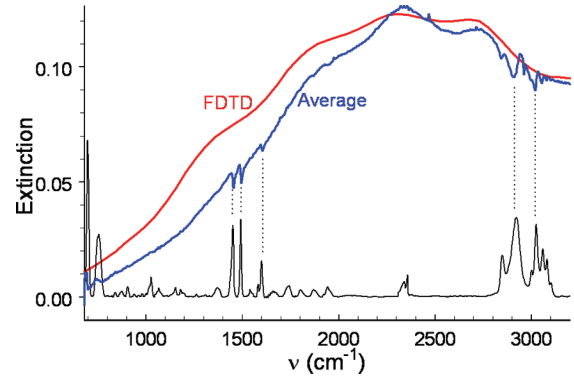


**Figure 6.** Average extinction spectra of 16 individual, 5 $\mu$m diameter, latex microspheres (blue) and the FDTD calculation without vibrations (red). An absorption spectrum of polystyrene (bottom, black) is also included, showing the position of the vibrations. Note how the vibrational features are smaller than the scattering and out-of-phase as compared with absorption.

absorptions and an interference pattern (suggesting perhaps that light is communicating between the holes). Despite the lack of extractable specifics, it is clear that the effect on transmission resonances of a single microsphere in a microhole is large.

## 5. FDTD Calculations of Mesh

On the basis of simulations of IR pulses impinging on gridded Ni metal mesh constructions and using brute force numerical integration of Maxwell's equations, transmission spectra at $k = 0$ (perpendicular incidence) were computed and compared to experimental zero-order transmission spectra (small range of $k$ values about $k = 0$) in Figure 9. The conditions of a standard desktop FTIR instrument are easier to model and quite different than with an IR microscope. Despite this, the FDTD calculations do a good job at reproducing the position and width of the primary transmission resonance at ~750 cm$^{-1}$. The simulation geometry is reasonably close to the experimental geometry (5.6 $\mu$m holes, 12.7 $\mu$m square lattice parameter, and ~2 $\mu$m of thickness). However, the actual shape of the holes is considerably different than the perfectly rectangular simulation in red. This and the small range of $k$ values about zero in the experimental data are likely important in the deviations between simulation and experiment, particularly at higher wavenumbers.

The next step placed spheres with an index of refraction similar to polystyrene ($n = 1.58$) into the hole and on the front surface of the metal mesh. These calculations were periodic for the mesh and so correspond to periodic arrangements of the dielectric spheres (not isolated spheres in holes as with section 4). The positions were chosen to avoid breaking the two-dimensional symmetry of the mesh (in which case, the primary transmission resonance splits into several peaks). One simulation has a 5.0 $\mu$m diameter sphere in the center of each hole and another has each sphere on the front surface centered between four holes. The corresponding transmission spectra are shown in Figure 10. A microsphere in the hole produces a dramatically larger shift of the primary transmission resonance—even though it constitutes the same amount of material as the case of the sphere on the front surface. The transmission resonance without spheres occurs at 764 cm$^{-1}$ and can be expected to redshift to 484 cm$^{-1}$ if the mesh were completely immersed in polystyrene ($n = 1.568$). When latex spheres are added to the holes, the peak grows in transmission and redshifts to 675 cm$^{-1}$, which is 32% of the maximum possible shift. When the same latex

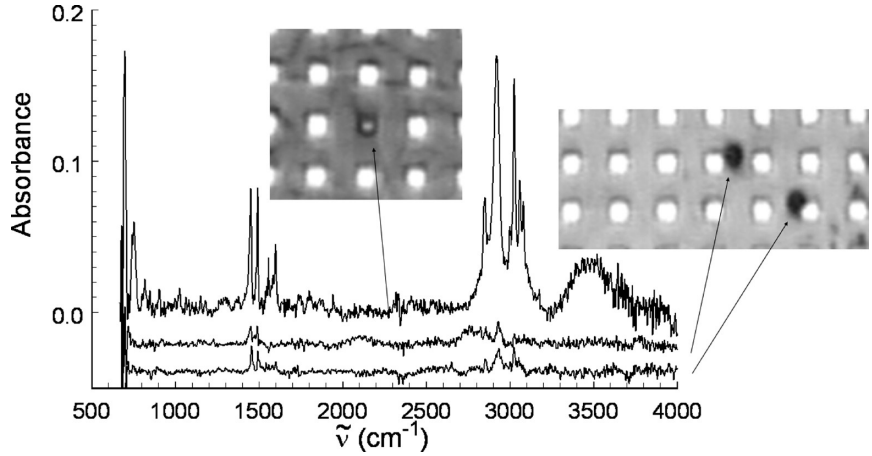


**Figure 7.** Absorption spectra of individual 5 $\mu$m diameter polystyrene spheres recorded for a sphere situated within a metal mesh hole (top trace and middle inset) and for two spheres outside of holes on the front mesh surface (bottom two traces and inset at right). Note that the scattering-dominated features of Figures 3, 5, and 6 are gone and the vibrational features occur totally in absorption. Absorption for a sphere within the hole is considerably stronger than for spheres not in the holes.

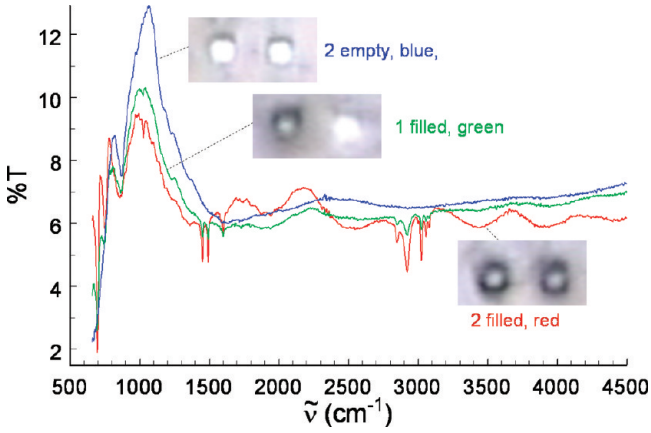


**Figure 8.** IR $\mu$scope transmission spectra of a 26 $\mu$m × 13 $\mu$m window (optical images inset) with two mesh holes that are empty (blue trace), one hole filled with a microsphere (green trace), and both holes filled with microspheres (red). Conditions: 400 scans, 4 cm$^{-1}$ resolution, and a single MCT detector.

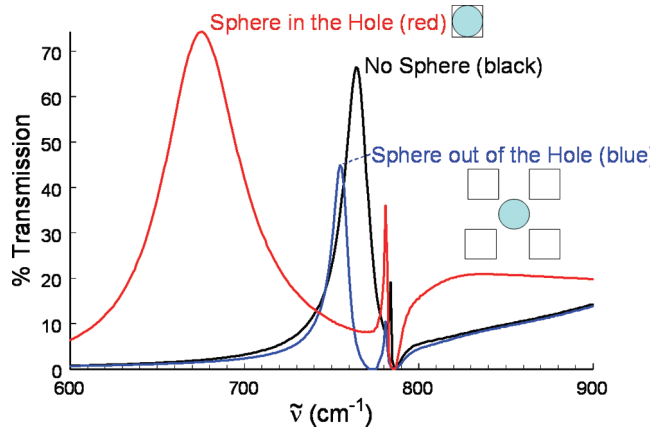


**Figure 10.** Transmission spectra at $k = 0$ from FDTD simulations of a blank mesh (black), one with a latex sphere filling and centered in the hole (red), and one with the latex sphere on the front surface between four holes.

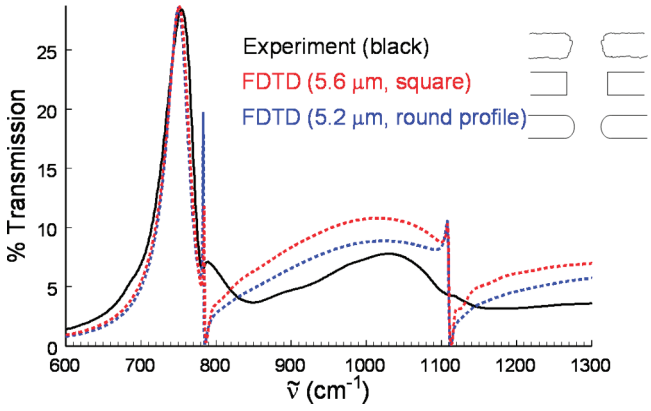


**Figure 9.** Transmission spectra at $k = 0$ from FDTD simulations compared to experiment (black trace). The red trace is a calculation based on a perfectly rectangular approximation to the experimental mesh. The blue trace shows the effect of a smaller hole diameter and rounding of the shape of the holes. The calculated intensities overestimate the experimental value and were scaled to experiment.

spheres are added on the front surface, symmetrically between four holes, the peak attenuates and shifts to 755 cm$^{-1}$ which is only 1.9% of the maximum shift. Clearly, there is considerably more response to material in the holes.

Finally, an attempt was made to address the effect on vibrational absorptions by adding a single vibrational term to the dielectric function of the polystyrene as

$$\varepsilon = 1.568^2 + \frac{\varepsilon_L \tilde{\nu}_0^2}{\tilde{\nu}^2 - \tilde{\nu}_0^2 + i\gamma\tilde{\nu}} \qquad (1)$$

where $\varepsilon_L = 0.004$ (a line strength), $\tilde{\nu}_0 = 700$ cm$^{-1}$, and $\gamma = 15$ cm$^{-1}$. The resulting $k = 0$ transmission spectra obtained with the vibrational term (solid traces) and without (dotted traces) are shown at the top of Figure 11. The traces without the vibrational term were used as backgrounds to obtain the absorbance line shapes presented at the bottom of Figure 11. The absorbance of the latex sphere in the hole is 11 times greater than the absorbance of a latex sphere out of the hole positioned symmetrically between four holes. The position of a vibration relative to a strong transmission resonance can make a significant contribution to the intensity of absorption.

## 6. Conclusion

Experimental IR microscope investigations on single microspheres and FDTD simulations on arrays of microspheres show that microspheres in the holes have a much stronger effect than those outside of the holes. The plasmonic transmission reso-

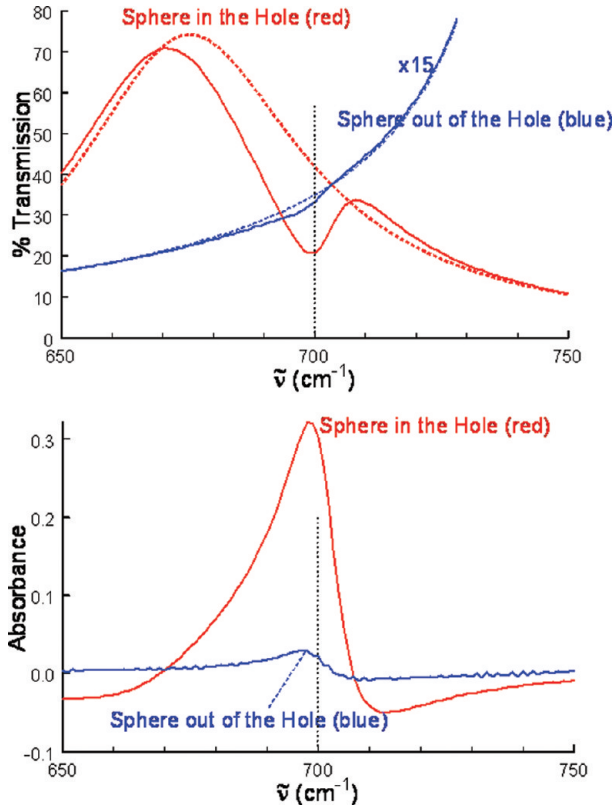


**Figure 11.** Effect of adding a vibrational term at 700 cm$^{-1}$ to the dielectric function of latex for the latex microsphere in the hole (red, solid trace) and on the front surface symmetrically between four holes (blue, solid trace). The dotted transmission curves are without the vibrational term and were used as backgrounds to calculate the absorption spectra below.

nances are shifted more and the IR vibrational absorption spectra are stronger when the microspheres are in the holes. Consider that some of the light incident on mesh hits metal and travels to the hole, some hits within the hole, some goes through the hole, and almost none goes through the metal (2 $\mu$m thick). Consequently, a portion of the spectroscopic enhancement is simply due to the fact that all of the light goes through the hole. Placement of the sample within the hole exposes that sample to more light than samples outside of the hole. On the other hand, our calculations also show that vibrational features near transmission resonances will have enhancement, which could be more than an order of magnitude on resonance. Both of these factors are likely important in the observed IR spectroscopic enhancements of samples on mesh.[18] It is clearly important to distinguish whether the sample is in or outside of the holes when considering the nature of spectroscopic enhancements for molecules on metal films with arrays of subwavelength holes.

The placement of a 5 $\mu$m diameter dielectric sphere within a square hole of a metal film of only 2 $\mu$m thickness produces an interesting optical construction where the equator of the sphere experiences a belt of metal. This arrangement reduces Mie scattering and the effect of scattering on vibrational line shapes, producing a pure vibrational absorption spectrum. This stands in contrast to the data of an individual sphere on ZnSe, which would require a Kramers−Kronig analysis to extract such absorption information. It is particularly interesting to us to consider two microspheres in adjacent holes—a case in between the single sphere and periodic arrangements studied herein. The extra interference pattern in the corresponding transmission trace of Figure 8 gives rise to curiosity about whether this arrangement can enhance plasmonic transmission between holes. If so, then such a construction might be considered a microsized plasmonic sensor or microspectrometer for microparticles caught between the spheres. Future work will investigate this as well as the details of enhancement regarding specific positions within the holes.

**Acknowledgment.** We thank the National Science Foundation for support of this work under Grant Nos. CHE 0848486 and CHE-0639163.

## References and Notes

(1) Ishikawa, H.; Tamaru, H.; Miyano, K. *J. Opt. Soc. Am. A* **2000**, *17*, 802–813.
(2) Barber, P. W., Chang, E., Eds. *Optical Effects Associated with Small Particles*; World Scientific Publishing Co. Pte. Ltd.: Singapore, 1988.
(3) Haynes, C. L.; Van Duyne, R. P. *J. Phys. Chem. B* **2001**, *105*, 5599–5611.
(4) Halteen, J. C.; Van Duyne, R. P. *J. Vac. Sci. Technol., A* **1995**, *13*, 1553–1558.
(5) Grudinkin, S. A.; Perova, T. S.; Moore, R. A.; Rakovich, Y. P.; Golubev, V. G.; Feoktistov, N. A. *Opt. Mater. (Amsterdam, Neth.)* **2007**, *29*, 983–986.
(6) Yamamoto, Y.; Slusher, R. E. *Phys. Today* **1993**, *46*, 66–73.
(7) Garcia-Vidal, F. J.; Martin-Moreno, L.; Pendry, J. B. *J. Opt. A: Pure Appl. Opt.* **2005**, *7*, S97–S101.
(8) Fang, N.; Liu, Z.; Yen, T.-J.; Zhang, X. *Opt. Express* **2003**, *11*, 682–687.
(9) Fang, N.; Zhang, X. *Appl. Phys. Lett.* **2003**, *82*, 161–163.
(10) Degiron, A.; Lezec, H. J.; Yamamoto, N.; Ebbesen, T. W. *Opt. Commun.* **2004**, *239*, 61–66.
(11) Barnes, W. L.; Dereux, A.; Ebbesen, T. W. *Nature* **2003**, *424*, 824–830.
(12) Genet, C.; Ebbesen, T. W. *Nature* **2007**, *445*, 39–46.
(13) Zhang, D.; Wang, P.; Jiao, X.; Tang, L.; Lu, Y.; Ming, H. *Wuli* **2005**, *34*, 508–512.
(14) Martin-Moreno, L.; Garcia-Vidal, F. J. *Adv. Solid State Phys.* **2004**, *44*, 69–80.
(15) Barnes, W. L.; Dereux, A.; Ebbesen, T. W. *Nature* **2003**, *424*, 824–830.
(16) Coe, J. V.; Heer, J. M.; Teeters-Kennedy, S.; Tian, H.; Rodriguez, K. R. *Annu. Rev. Phys. Chem.* **2008**, *59*, 179–202.
(17) Gordon, R.; Brolo, A. G.; Sinton, D.; Kavanagh, K. L. *Laser Photonics Rev.*, published online May 11, http://dx.doi.org/10.1002/lpor.200810079.
(18) Coe, J. V.; Rodriguez, K. R.; Teeters-Kennedy, S.; Cilwa, K.; Heer, J.; Tian, H.; Williams, S. M. *J. Phys. Chem. C* **2007**, *111*, 17459–17472.
(19) Hinds, W. C. *Aerosol Technology: Properties, Behavior, And Measurement of Airborne Particles*; J. Wiley: New York, 1982.
(20) Dumas, P.; Carr, G. L.; Williams, G. P. *Analusis* **2000**, *28*, 68–74.
(21) Raynal, P. I.; Quirico, E.; Borg, J.; Deboffle, D.; Dumas, P.; d'Hendecourt, L.; Bibring, J. P.; Langevin, Y. *Planet. Space Sci.* **2000**, *48*, 1329–1339.
(22) Raynal, P. I.; Quirico, E.; Borg, J.; Deboffle, D.; Dumas, P.; d'Hendecourt, L.; Bibring, J. P.; Langevin, Y. *Planet. Space Sci.* **2000**, *48*, 1329.
(23) Ferreira, J.; Santos, M. J. L.; Rahman, M. M.; Brolo, A. G.; Gordon, R.; Sinton, D.; Girotto, E. M. *J. Am. Chem. Soc.* **2009**, *131*, 436–437.
(24) Garcia de Abajo, F. J.; Gomez-Medina, R.; Saenz, J. J. *Phys. Rev. E* **2005**, *72*, 4.
(25) Strelniker, Y. M.; Stroud, D.; Voznesenskaya, A. O. *Eur. Phys. J. B* **2006**, *52*, 1–7.
(26) Williams, S. M.; Stafford, A. D.; Rodriguez, K. R.; Rogers, T. M.; Coe, J. V. *J. Phys. Chem. B* **2003**, *107*, 11871–11879.
(27) Yee, K. Antennas and Propagation. *IEEE Trans.* **1966**, *14*, 307.
(28) Palik, E. D. *Handbook of Optical Constants of Solids*; Academic Press: San Diego, CA, 1998; Vol. 3.
(29) van de Hulst, H. C. *Light Scattering by Small Particles*; Dover: New York, 1981.
(30) van de Hulst, H. C. *Light Scattering by Small Particles*; John Wiley and Sons: New York, 1958.
(31) Dunder, T.; Miller, R. E. *J. Chem. Phys.* **1990**, *93*, 3693–3703.
(32) Christiansen, C. *Ann. Phys.* **1884**, *259*, 298–306.

JP908897Z